International Journal of Mass Spectrometry 302 (2011) 76–84

Contents lists available at ScienceDirect

International Journal of Mass Spectrometry

journal homepage: www.elsevier.com/locate/ijms

Analysis of human ferrochelatase iron binding via amide hydrogen/deuterium exchange mass spectrometry

Awuri P. Asuru, Laura S. Busenlehner*

Department of Chemistry, The University of Alabama, Tuscaloosa, AL 35487, USA

ARTICLE INFO

Article history:
Received 31 May 2010
Received in revised form 29 July 2010
Accepted 2 August 2010
Available online 10 August 2010

Keywords:
Ferrochelatase
Hydrogen/deuterium exchange mass spectrometry
Protein dynamics
Heme synthesis

ABSTRACT

Human ferrochelatase (E.C. 4.99.1.1) is a membrane-associated enzyme that catalyzes the last step in the heme biosynthetic pathway, the insertion of ferrous iron into protoporphyrin IX. Crystallographic structures have revealed that protoporphyrin binds in a cleft between two domains; however, the entry pathway and location of the iron binding site(s) is still contested. In an effort to address this issue, the structural elements involved in binding substrate iron were studied by amide hydrogen/deuterium exchange mass spectrometry. The deuterium incorporation rates into the backbone of apo- and iron-ferrochelatase in the absence of porphyrin substrate were measured. For the first time, it is demonstrated how the binding of ferrous iron specifically modulates ferrochelatase structure in solution. The distinct regions affected by the presence of iron provide insight into the mechanism by which iron is transported to the active site.

1. Introduction

Ferrochelatase (E.C. 4.99.1.1) catalyzes the terminal step of heme biosynthesis by catalyzing the insertion of ferrous iron in protoporphyrin IX to form protoheme IX (Fig. 1) [1]. The newly formed heme is incorporated into various proteins and enzymes that perform vital functions in the human body such as cellular respiration and the transport of electrons and oxygen. The disruption of the heme biosynthetic pathway leads to several disorders and diseases. Mutations resulting in the diminished activity of ferrochelatase cause the inherited disorder erythropoietic protoporphyria (EPP) [2,3]. Individuals with EPP experience painful dermatologic photosensitivity due to tissue damage that occurs when accumulated protoporphyrin IX in the skin is exposed to visible light [4].

Human ferrochelatase exists as an inner mitochondrial membrane-associated homodimeric enzyme *in vitro* and each monomer contains a [2Fe–2S] cluster [5]. X-ray crystallographic structures of ferrochelatase from different organisms have been solved and all structures displayed two similar Rossmann-type domains with a porphyrin binding cleft between them [6–11]. In all published crystallographic structures of ferrochelatases, only the 1.7 Å resolution structure from *Bacillus subtilis* contained the Fe(II) substrate [11]. Crystallographic evidence with surrogate metals such as Hg(II) and Co(II) suggest there is an outer metal binding site (His231, Asp383) near the matrix-exposed surface of ferrochelatase as part of a channel leading from the surface of the protein to the catalytic site where protoporphyrin is bound [7,9]. In this pocket, His263 is suggested to abstract a proton from the porphyrin macrocycle during catalysis [12]. However, mutational studies of the human and yeast enzymes and the recent structure of *B. subtilis* ferrochelatase support that this invariant His residue is involved in Fe(II) binding and insertion into protoporphyrin IX [9,11,13]. Thus, position of the catalytic metal binding site in human ferrochelatase and the pathway involved in metal insertion is still a matter of debate.

Structures of various ferrochelatases with and without substrate metals do not show remarkable changes in conformation upon metal coordination in the absence of porphyrin [7,9]. This could be the result of soaking apo-ferrochelatase crystals in a metal solution and not having initially crystallized the Fe(II)-bound form of the enzyme. In addition, these static structures give little insight into the structural dynamic component of catalysis for most enzymes [14]. Recent structures indicate that porphyrin binding to ferrochelatase in the absence of iron causes the active site "mouth" to close, resulting in the reorientation of the binding pocket [10,12,15]. Many lines of evidence support that protein dynamics are critical to controlling steps in catalysis such as substrate binding or product release [15–18]. Thus amide hydrogen/deuterium exchange mass spectrometry (H/D-exchange MS)[1]

Abbreviations: HD-exchange MS, hydrogen/deuterium exchange mass spectrometry; β-ME, β-mercaptoethanol; CHAPS, 3-[(3-Cholamidopropyl) dimethylammonio]-2-hydroxy-1-propanesulfonate; MPIX, mesoporphyrin IX; ddH_2O, doubly distilled H_2O; D_2O, deuterium oxide.

* Corresponding author. Tel.: +1 205 348 0269.
E-mail addresses: apasuru@crimson.ua.edu (A.P. Asuru), LSBusenlehner@bama.ua.edu (L.S. Busenlehner).

1387-3806/$ – see front matter © 2010 Elsevier B.V. All rights reserved.
doi:10.1016/j.ijms.2010.08.004

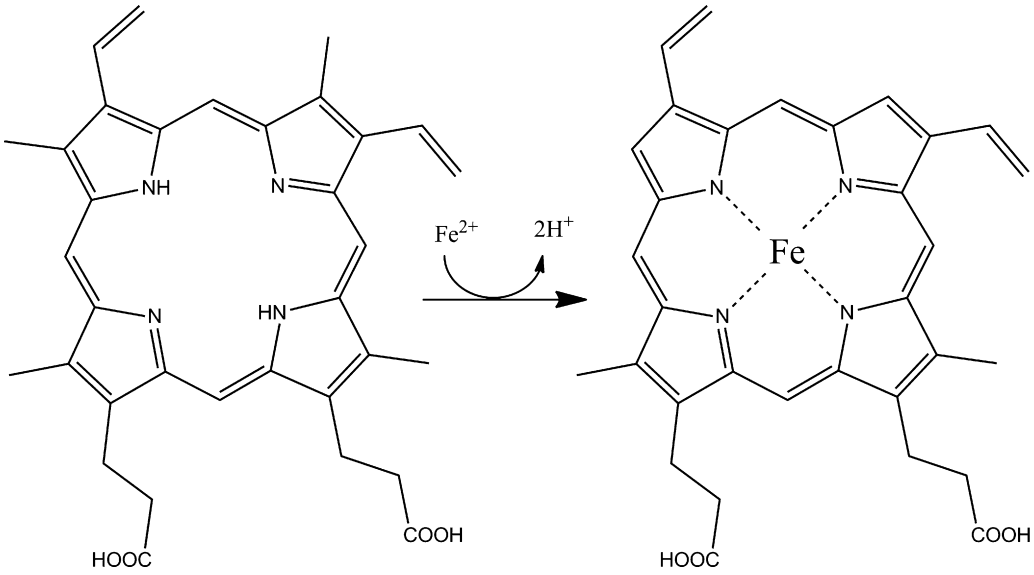

Fig. 1. Ferrochelatase reaction. Ferrochelatase (E.C. 4.99.1.1) catalyzes the formation of heme (protoheme IX) by insertion of ferrous iron into protoporphyrin IX.

presents an excellent method to probe the structural dynamics of ferrochelatase in relation to its catalytic mechanism [14]. Here, the technique was used to investigate the regions of the enzyme that experience changes in structure and/or dynamics in the presence of ferrous iron substrate. These studies provide structural insight into how ferrochelatase binds iron and transports it to the active site in the absence of protoporphyrin IX. In addition, this work has indicated new regions of ferrochelatase as of yet unexplored in terms of metal binding. The significance of these results is discussed.

2. Materials and methods

2.1. Protein expression and purification

Escherichia coli HB101 cells were transformed with pHisTF20E provided by Dr. Harry Dailey (University of Georgia) and plated on LB agar with 100 μg/mL ampicillin [19]. A single colony was used to inoculate 2 L of Circlegrow medium (Bio101, Vista, CA) that was supplemented with 50 μg/mL carbenicillin. The cells were incubated at 37 °C and 225 rpm until the cells reached stationary phase. The harvested cells were stored at a temperature of −20 °C.

The cells were resuspended in 10 mL of solubilization buffer (Buffer S) composed of 50 mM sodium phosphate (pH 8.0), 300 mM NaCl, 10 mM β-mercaptoethanol (β-ME), 10 mM imidazole, and 3% CHAPS. Phenylmethanesulphonyl fluoride (1 mg/mL) and lysozyme (1 mg/mL) were then added and the homogenate was lysed with a Branson Sonifier 250 (Danbury, CT) on ice with 30 s pulses at 60% saturation power. Following centrifugation at 14,000 × *g* for 15 min at 4 °C, the lysis supernatant was diluted with solubilization buffer (no CHAPS) to lower the CHAPS concentration to 1% for metal affinity chromatography.

Ferrochelatase was purified using 1 mL packed Ni-NTA Superflow resin (5 Prime, Gaithersburg, MD) equilibrated with Buffer S (10 mM imidazole). The resin and lysis supernatant were combined and allowed to incubate overnight at a temperature of 4 °C. Following incubation, the resin was loaded into a column and the eluant collected. The resin was washed with ∼1 mL of Buffer S, then ∼5 mL of Buffer S with 50 mM imidazole. Ferrochelatase was eluted with ∼2 mL of Buffer S plus 200 mM imidazole. Following purification, an additional 20 mM β-ME was added to the elution. Purified ferrochelatase was dialyzed against 2 L of chelexed 25 mM HEPES (pH 7.4), 100 mM NaCl, 20 mM β-ME, and 0.1% CHAPS at 4 °C. The concentration of ferrochelatase was estimated at 278 nm (ε_{278} = 46,910 M^{-1} cm^{-1}) and the percentage of bound [2Fe–2S] cluster was estimated by the absorbance at 330 nm (ε_{330} = 12,000 M^{-1} cm^{-1}) [19]. The iron content of purified apoferrochelatase was measured by atomic absorption spectroscopy and found to be 1.8 ± 0.1 mol iron per mol ferrochelatase, as expected if each monomer contains the [2Fe–2S] cluster.

2.2. Ferrochelatase activity measurements

The activity of ferrochelatase in the zwitterionic detergent CHAPS was accessed since previous purification schemes used the anionic detergent cholate which is not amenable to electrospray ionization mass spectrometry [19–21]. Activity measurements monitored the conversion of mesoporphyrin IX dihydrochloride (MPIX; Frontier Scientific, Logan, UT) to protoporphyrin IX through a decrease of the Soret band at 496 nm [22]. A 0.78 mM MPIX stock solution was made by dissolving 2.5 mg MPIX with 30 μL 2N ammonium hydroxide, 500 μL 10% Triton X-100 in 4.5 mL doubly distilled H_2O (ddH_2O). A 1 mM ferrous ammonium sulfate solution with 5 mM ascorbate in ddH_2O was prepared immediately prior to activity measurements. The assay mixture had a total volume of 1 mL and contained 100 mM Tris–HCl (pH 8.0), 0.5% Tween-20, 10 μM MPIX, 10 mM β-ME and 0.5 μM ferrochelatase at room temperature. Ferrous ammonium sulfate (0.5–30 μM) was added to start the reaction. The initial velocities were used to generate the Michaelis–Menten plot which yielded K_m^{Fe} = 5.8 ± 1.9 μM and a k_{cat} = 1.11 ± 0.04 min^{-1}, which are similar to reported values with sodium cholate as the detergent [22].

2.3. Pepsin peptide mapping

The protein sample for digestion contained ∼1 μM ferrochelatase in 50 mM potassium phosphate buffer (pH 2.3). Approximately 40 μg of porcine pepsin (Sigma Aldrich, St. Louis, MO) was added and the sample was incubated on ice for either 5 or 8 min. The 8 min digest did not yield a significantly different digestion result. The pepsin digest (20 μL) was loaded onto a Phenomenex microbore 1 mm × 50 mm C18 reverse-phase column (Torrence, CA) that had been equilibrated with HPLC-grade aqueous solvent (98% H_2O, 2% acetonitrile, 0.4% formic acid). The column was washed with aqueous solvent for 2 min at 60 μL/min

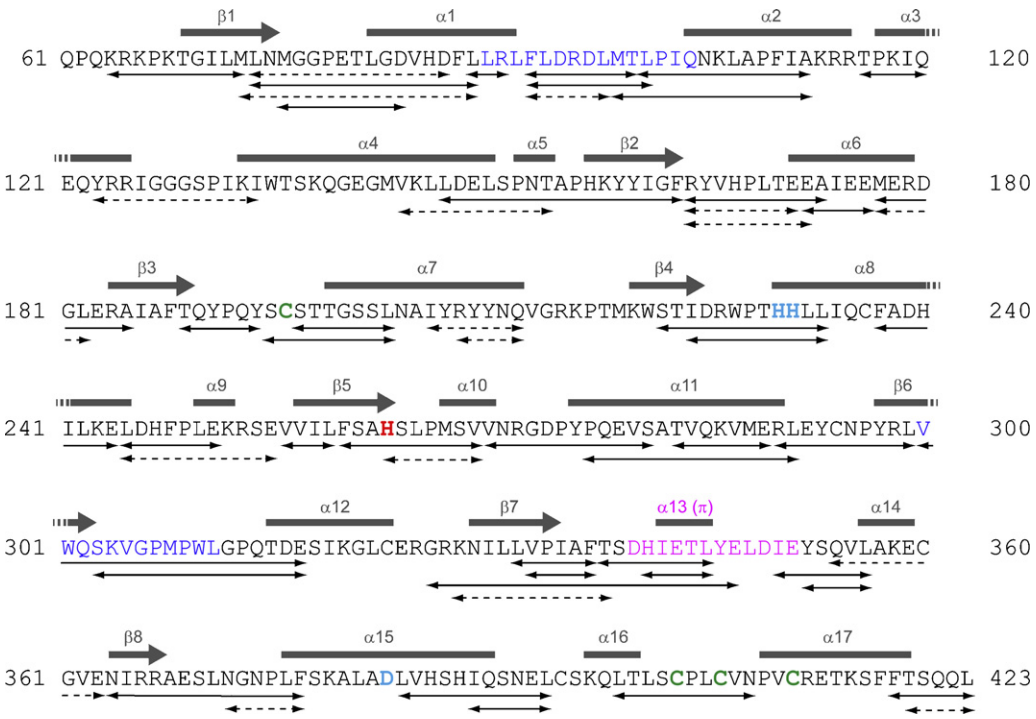

Fig. 2. Pepsin peptide map of ferrochelatase. Ferrochelatase in 0.1% CHAPS (~1 μM) was digested with ~40 μg pepsin for 8 min on ice (pH 2.3). Peptides were separated by reversed-phase HPLC and eluted peptides were introduced into the ion trap mass spectrometer via electrospray where they were fragmented by CID. The peptides identified cover ~83% of the amino acid sequence; however, the peptides indicated by solid arrows were the ones used for H/D-exchange analysis due to their abundance, signal-to-noise, and isotopic envelopes. The practical sequence coverage was 74%. The secondary structure labeled above the amino acid sequence is based on [7]. The upper and lower lips are in blue, the active site residue His263 is in red, the anionic channel is in magenta, the initial metal binding residues from the crystal structure [7] are in cyan, and the cysteines that ligate the [2Fe–2S] cluster are in green.

to remove early eluting salts, which were diverted from the mass spectrometer. The peptides were eluted with a 30 min linear gradient of 0–80% HPLC-grade organic solvent (98% acetonitrile, 2% H_2O, and 0.4% formic acid) at 60 μL/min. At the end of every run, the column was washed extensively with a isopropanol-containing solvent to remove detergent (40% 2-propanol, 50% acetonitrile, 0.4% formic acid in water), which was diverted to waste. Peptides were sequenced using a HCT Ultra PTM Discovery ion trap mass spectrometer (Brüker Daltonics, Billerica, MA) by electrospray ionization in positive-ion mode by data-dependent tandem MS/MS collision-induced dissociation. The capillary temperature was 250 °C and the SmartFrag™ algorithm was used to optimize fragmentation. The amino acid sequence of the peptides were determined by comparison to the *in silico* CID fragmentation patterns for ferrochelatase generated by the program MS-Product [23]. The full peptide map is shown in Fig. 2 which has approximately 74% sequence coverage by the peptides used reproducibly for H/D exchange.

2.4. Hydrogen/deuterium exchange mass spectrometry

Deuterium exchange was initiated by the addition of 5 μL of ~20 μM apo or Fe(II)-ferrochelatase to 45 μL of D_2O. For iron samples, 1 mM ferrous ammonium sulfate was prepared fresh with degassed chelexed-water and 5 mM ascorbic acid and assayed for Fe(II) using ferrozine [22]. Approximately 1.5 molar equivalents of iron were added to 5 μL ferrochelatase aliquots and were purged with N_2 for 2–3 min, then sealed. D_2O was added separately to each aliquot. The deuterium-protein samples were incubated at 23 °C for 15 s to 2 h, after which the exchange reaction was quenched by addition of 50 μL of quench buffer [0.1 M potassium phosphate (pH 2.3) in H_2O; 0 °C] and immediately transferred to an ice bath. After 25 s, 2 μL of 20 μg/μL pepsin in 10 mM potassium phosphate, pH 7.0 was added (40 μg), and the digestion proceeded for 5 min. The peptide digests were individually loaded onto a 1 mm × 50 mm C18 reverse-phase column and eluted with a linear gradient (0–80% organic solvent B) over 12 min at 60 μL/min and monitored by electrospray ionization in positive-ion mode (300–1600 m/z) with a capillary temperature of 190 °C. All protein samples for the H/D were prepared individually and run on the same day.

To determine the extent of deuterium incorporation that occurred after the acidification and during the pepsin digestion, a zero-time control ($m_{0\%}$) was performed [14]. Ferrochelatase (5 μL of ~20 μM) was added to 50 μL of quench buffer at 0 °C, followed by the addition of 45 μL of D_2O. Pepsin was subsequently added (40 μg), and the protein was digested for 5 min on ice, as described. The amount of deuterium that is lost during the HPLC chromatography step can also be determined. A completely deuterated protein sample ($m_{100\%}$) was prepared by combining 5 μL of ~20 μM ferrochelatase with 45 μL of D_2O. Samples were then allowed to incubate for approximately 4 h at 45 °C. After incubation, amide hydrogen exchange was quenched with the addition of 50 μL of 0.1 M potassium phosphate buffer (pH 2.3) in D_2O and allowed to incubate at 45 °C for 2 h. The incubation in deuterated quench buffer allowed for better deuterium incorporation, as compared to further incubation at pH 7. Pepsin was then added and samples were separated as above.

Peptide ions were located by mass searching, yielding the chromatographic retention profile for each ion. The scans contained within the extracted chromatographic ion profile were averaged to produce a composite spectrum for each ion. MagTran 1.0 beta 9 software developed by Zhang and Marshall was used to determine the centroid (m_t) of the given composite isotope envelope [24]. For multiply charged peptides, isotopic envelopes from different charge state ions were averaged when appropriate. The deuterium content of partially deuterated peptides (D) was corrected for the

gain ($m_{0\%}$) and loss ($m_{100\%}$) of deuterium during analysis using

$$D = N\left(\frac{m_t - m_{0\%}}{m_{100\%} - m_{0\%}}\right) \quad (1)$$

where $m_{0\%}$, m_t, and $m_{100\%}$ are the average molecular masses of the peptide in the nondeuterated, the partially deuterated at time t, and the fully deuterated control samples, respectively [25]. N is the total number of exchangeable peptide amide protons less one for the N-terminal amide proton and any proline residues. The amount of deuterium incorporated in each peptide was averaged from two or three independent kinetic runs and plotted as a function of time. The resulting progress curve for each peptide was fit using KaleidaGraph (Synergy Software) to the sum of first-order rate terms,

$$D = N - A_1e^{-k_1t} - A_2e^{-k_2t} - A_3e^{-k_3t} \ldots - A_ne^{-k_nt} \quad (2)$$

where D is the number of incorporated deuteriums incorporated, N is the total number of exchangeable sites, A_n is the number of amide protons that exchange at a given rate constant, k_n, during the time allowed for isotopic exchange, t. The kinetic profiles were fit to single or double exponential equations as appropriate. The H/D incorporation kinetic profiles for all identified ferrochelatase peptides can be found in Supplementary Content.

3. Results

3.1. Ferrochelatase stability

Several problems were addressed before H/D-exchange MS was used to study human ferrochelatase. The first problem is that existing purification protocols for ferrochelatase require the use of sodium cholate, a detergent incompatible with mass spectrometry [20]. While removal methods exist for cholate detergents, the inclusion of such a step only adds to the time required to process the sample after H/D-exchange which can lead to progressive loss of the deuterium label. The second problem is that ferrochelatase in sodium cholate begins to precipitate shortly after being purified [19]. Human ferrochelatase is unstable due to its labile [2Fe–2S] cluster, which is anchored to the enzyme by four cysteine residues [6]. After aerobic purification, the cysteine residues can oxidize and release the [2Fe–2S] cluster, causing ferrochelatase to precipitate. After testing detergents compatible with mass spectrometry, CHAPS was best at solubilizing ferrochelatase, while retaining full activity as compared to the enzyme in sodium cholate. Also, the amount of CHAPS in the sample after H/D exchange and acidification is ~0.005%, which is lower than the concentration of detergent which causes signal suppression [20,21]. The CHAPS-solubilized sample exhibited a red-orange color with a broad absorbance features at between 300 and 500 nm characteristic of the [2Fe–2S] cluster [19]. Most importantly, CHAPS-solubilized ferrochelatase in the presence of reducing agent retained the [2Fe–2S] cluster over 3 weeks at 4 °C with little precipitation. It was essential for the structural analysis by H/D-exchange MS to stabilize ferrochelatase. Using UV–vis spectroscopy there was negligible base line shift in the visible region over a 2 h H/D exchange time course and our enzymatic assay measurements indicate that <5% of the activity was lost after a 2 h incubation under N_2 at 25 °C. UV–vis spectroscopy also confirmed that the purified ferrochelatase did not contain a porphyrin molecule in the active site, as determined by the lack of a characteristic Soret band [26]. For H/D-exchange MS, ferrochelatase in the absence of its substrate PPIX was chosen for characterization to eliminate enzyme turnover upon the addition of iron.

3.2. Characterization of apo ferrochelatase

The kinetics of backbone amide H/D exchange is dependent on a variety of factors including protein structure, pH, and adjacent

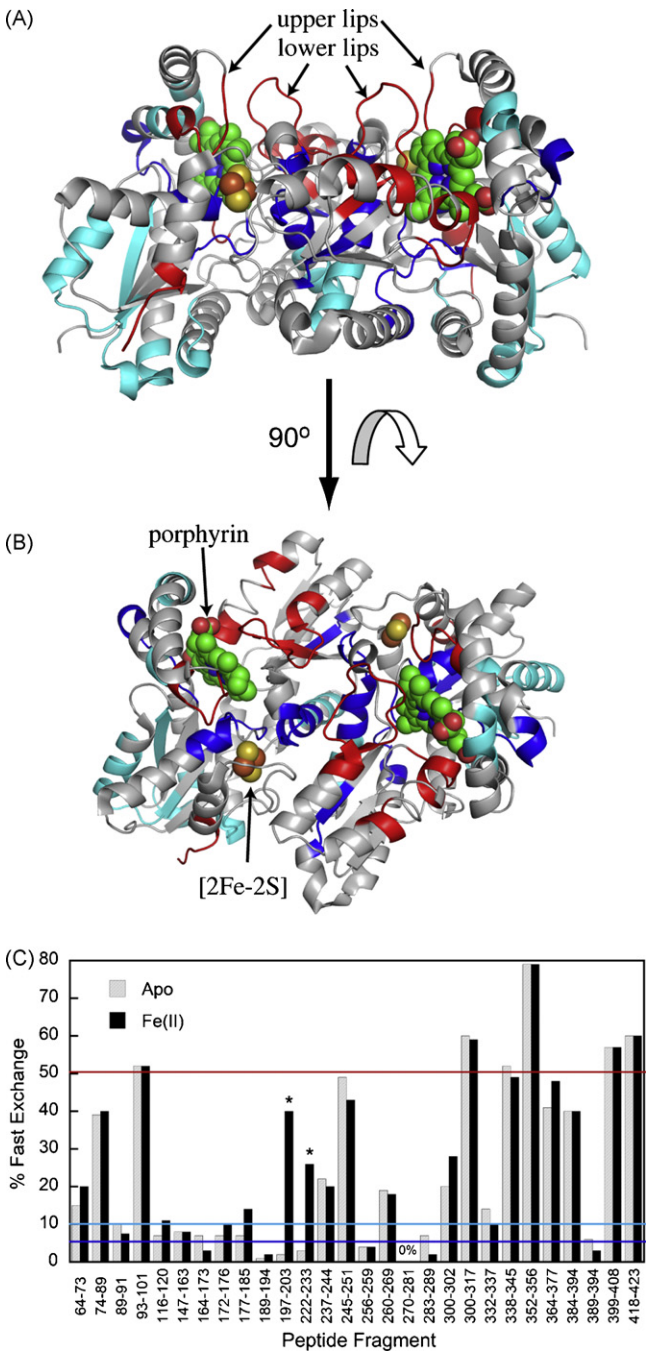

Fig. 3. Solvent accessibility maps. (A) Shown is a side-on view of the apo-ferrochelatase dimer with peptides indicated. Protoporphyrin (green) is shown for clarity, but the enzyme form for H/D-exchange MS did not contain the substrate. The red areas are peptides most accessible to deuterium (≥50% exchange) and include peptides 93–101, 300–317, 338–345, 352–356, and 418–413. The cyan areas are mostly protected from deuterium (≤10% exchange) and include peptides 89–91, 116–120, 147–163, 172–185, 283–289, and 389–394. The blue areas are highly protected from deuterium (≤5% exchange) and include peptides: 76–84, 189–194, 197–203, 222–233, 256–259, and 270–281. (B) Top view (rotated 90°). (C) Shown is a bar chart with the percentage of deuterium incorporation for apo- and Fe(II)-ferrochelatase. Peptides above the 50% line are colored red in A and B. Those below the 10% line are colored cyan and those below the 5% lines are in blue. The asterisks indicate the two peptides with significant changes in solvent accessibility upon addition of iron (197–203 and 222–233). Structures were made with PyMOL [38] using PDB 2QD1. A movie of the solvent accessibility mapped on the structure can be found in Supplementary Content (Movie S1). (For interpretation of the references to color in this figure legend, the reader is referred to the web version of the article.)

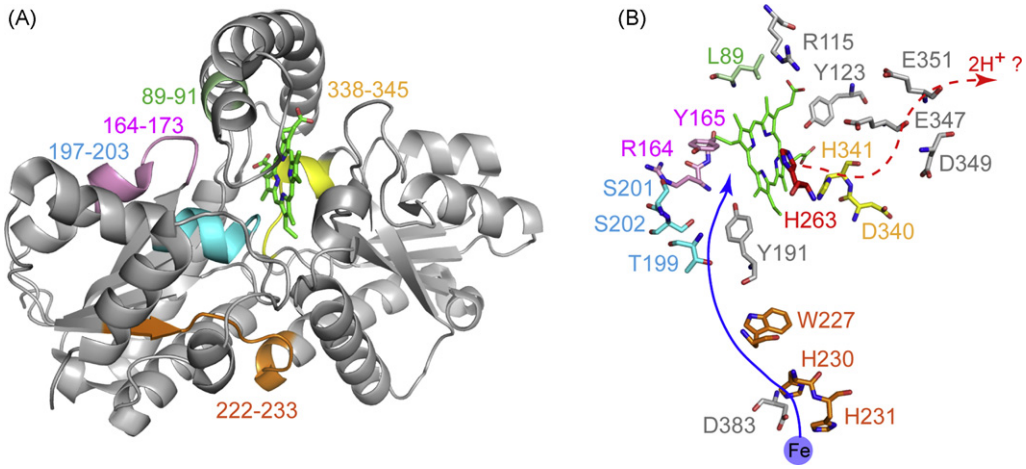

Fig. 4. Regions with altered H/D exchange kinetics. (A) Shown is the structure of monomeric ferrochelatase displaying changes in deuterium incorporation with addition of iron. Protoporphyrin (green) is shown for clarity, but the enzyme form for H/D-exchange MS did not contain the substrate. The peptides are: 89–91, light green; 164–173, pink; 197–203, cyan; 222–233, orange; 338–345, yellow. (B) Individual residues important to the mechanism of ferrochelatase are shown in stick format with the cartoon structure of ferrochelatase removed for clarity. The orientation was adjusted for clarity and is not the same as in (A) but the backbone coloring scheme remains the same. His263 is in red. The one projected channel for Fe(II) from the initial binding site is shown in blue [12,31]. The possible exit pathway for the 2 protons is indicated in red. A movie of the pepsin peptides mapped on the structure can be found in Supplementary Content (Movie S2). (For interpretation of the references to color in this figure legend, the reader is referred to the web version of the article.)

amino acid side-chains of the amide group [27,28]. In general, the amount of deuterium incorporation within the first 15 s of a H/D-exchange time course experiment can provide a rough estimate of the relative accessibility of backbone amides to OD^- during base catalyzed exchange ($k_{ex} \geq 10\,s^{-1}$ at pH 7, 25 °C) [29,30]. As expected, the most protected regions from deuterium were at the dimer interface of apo-ferrochelatase (Fig. 3, blue), which has an extensive hydrogen bonding network, and also near the [2Fe–2S] cluster [7]. Other areas with minimal deuterium incorporation include the bottom of the porphyrin binding cleft and the β–α–β motif of the N-terminal Rossmann domain (Fig. 3, cyan). The most solvent accessible areas of ferrochelatase are found in the upper and lower hydrophobic "lips" of the active site pocket (Fig. 3, red) which are likely the sites for membrane association. These membrane-associated loops position the active site towards the hydrophobic membrane and allow the poorly soluble porphyrin substrate to enter and the heme product leave through the membrane [26]. The H/D exchange results are also consistent with the high crystallographic B factors observed for human ferrochelatase (PDB 2QD1) in sodium cholate [31]. Other accessible regions include the π-helix (α_{13}), which lines a solvent accessible path leading from the protein surface to the active site, and the C-terminal tail.

3.3. Changes in ferrochelatase structure and dynamics upon iron binding

In the presence of ferrous iron, the amount of deuterium incorporation in the fast phase is relatively similar to that of apo-ferrochelatase with the exception of two pepsin-generated peptides, 197–203 and 222–233 (Fig. 3C). Peptides 197–203 and 222–233 showed little to no on-exchange of deuterium in the fast phase in the metal free protein, but became more accessible in the iron-bound state with a 26% and 38% increase, respectively (Fig. 3C). These two regions form a putative channel for transporting iron from one proposed initial binding site exposed to the mitochondrial matrix (His230, His231, Asp383) to the active site pocket where protoporphyrin binds [7]. The increase in deuterium incorporation upon iron binding and transport indicates that the channel partially "opens" in response to iron, and exposes previously protected backbone amides to deuterium. It is interesting to note that there are no ferrochelatase peptides that become less accessible to D_2O upon addition of iron. This result is not unexpected since iron binding is unlikely to significantly protect amides from D_2O solvent [32,33].

There were a total of five ferrochelatase peptides from the pepsin digest with altered H/D-exchange time course kinetics upon addition of ferrous iron, including peptides 197–203 and 222–233 described above, along with 89–91, 164–173, and 338–345. All five peptide fragments are mapped on the monomeric structure of ferrochelatase in Fig. 4. As noted above, peptides 222–233 and 197–203 show a clear increase in the solvent accessibility in the presence of iron (Fig. 5A and B). In addition to the increased solvent accessibility, peptide 222–233 (Fig. 4, orange) maintains a steady level of deuterium incorporation over a 2-h incubation, indicating that only 3 of the 10 amide hydrogens are accessible to D_2O as compared to 2 hydrogens for the apo-enzyme. In both states, this suggests a lack of dynamic, local unfolding in this area. For peptide 197–203, which is farther up the putative iron channel and closer to the active site (Fig. 4, cyan), the amount of deuterium incorporated for both apo- and Fe(II)-ferrochelatase is similar after 2 h of incubation; however, the kinetic profiles are different (Fig. 5B). This peptide clearly shows an increased rate of deuterium exchange in the presence of iron which saturates at 4 out of the 6 backbone amides. This indicates that in the absence of iron, residues 197–203 reside in a solvent-protected environment that undergoes local dynamic unfolding which allow for deuterium exchange, but in the presence of iron, this area has much greater solvent (*i.e.*, D_2O) access and possibly increased dynamic motions.

In contrast, there are three peptides from the digest that display decreased deuterium incorporation as a function of time when comparing iron-bound ferrochelatase to the apo-form (Fig. 5C–E). Peptide 164–173 is located directly across from the substrate binding site (Fig. 3, pink) and contains two key residues hypothesized to play an important role in iron transport through the channel and metallation of substrate, Arg164 and Tyr165 [34]. This peptide is fairly inaccessible to D_2O in both the apo- and iron-bound enzyme as given by the lack of exchange by the 15 s time point (Fig. 5C). However, the rate of exchange for 4 of the 8 amides in the apo-enzyme is almost 4 times faster than that in the iron-bound state. This indicates a loss of dynamics the presence of iron. There is also a loss of dynamics for peptide 89–91 in the presence of iron (Fig. 5D). This small peptide is located in α_1-helix above the protoporphyrin binding site (Fig. 4, light green). While this area is somewhat pro-

Table 1
Rate constants and amplitudes for H/D exchange into selected peptides[a].

Peptide	Pre-exchanged[b] (%, $k > 4\,min^{-1}$)	Exchange, A1 (%)	Rate, k_1 (min^{-1})	Exchanged, A2 (%)	Rate, k_2 (min^{-1})[c]
89–91(2)					
Apo	~5	33.3 (±3.9)	0.7 (±0.2)	61.5 (±2.2)	0.011 (±0.001)
Fe(II)	~12	37.7 (±1.3)	0.035 (±0.005)	~50	$\leq 1 \times 10^4$
164–173 (8)					
Apo	~6	39.4 (±3.0)	0.22 (±0.05)	54.1 (±2.8)	$\leq 1 \times 10^4$
Fe(II)	~8	24.8 (±1.1)	0.06 (±0.01)	66.5 (±11.1)	$\leq 1 \times 10^4$
197–203 (6)					
Apo	~4	–	–	95.1 (±2.0)	$6.3\ (\pm 0.7) \times 10^3$
Fe(II)	~20	29.7 (±9.3)	1.4 (±0.6)	~50	$\leq 1 \times 10^4$
222–233 (10)					
Apo	~3	23.4 (±9.7)	1.6 (±0.9)	79.7 (±2.4)	$1.9\ (\pm 0.5) \times 10^3$
Fe(II)	~35	–	–	64.4 (±0.5)	$\leq 1 \times 10^4$
260–269 (8)					
Apo	~25	–	–	74.9 (±1.6)	$3.6\ (\pm 0.6) \times 10^3$
Fe(II)	~20	–	–	79.2 (±0.5)	$3.8\ (\pm 0.5) \times 10^3$
338–345 (7)					
Apo	~39	50.9 (±2.5)	0.40 (±0.04)	~10	$\leq 1 \times 10^4$
Fe(II)	~28	41.7 (±1.5)	1.5 (±0.2)	~30	$\leq 1 \times 10^4$

[a] Parameters obtained from fitting the H/D-exchange kinetics of Fig. 3 according to the single or double exponential expression of Eq. (2). The number in parentheses is the total number of exchangeable amide hydrogens.
[b] The amount of exchange before the first time point is estimated from the fit parameters and has a rate of exchange faster than $4\,min^{-1}$.
[c] The amount of deuterium in the slowest phase was determined from the fit when applicable. Otherwise the value was obtained by %A2 = 100% − %A1 − %pre-exchanged.

tected from deuterium exchange initially, the incorporation rate of one deuterium is almost 20 times slower with iron present and an additional amide is still unexchanged over 2 h, which in is contrast to apo-ferrochelatase which is almost fully deuterated at 2 h. This suggests that the backbone of this helical region is more rigid in iron-bound ferrochelatase. The third peptide, 338–345, is part of the π-helix (α_{13}) that forms the base of the porphyrin binding pocket (Fig. 4, yellow). In the presence of iron, an additional amide hydrogen is protected from deuterium exchange compared to apo-ferrochelatase; however, the rates of exchange for both states are similar (Fig. 5F). This may be the result of additional hydrogen-bonding in Fe(II)-ferrochelatase. Peptide 338–345 contains the key catalytic residues Glu343 and Asp340 which may be involved in abstracting two protons from the pyrrole during metal insertion [34]. This region could also form an anionic surface for the putative transport of protons out of the active site [12]. Alternatively, some research suggests that this anionic surface could be one route by which iron is translocated to the active site residue His263 [11]. It is also of interest that peptide 260–269 which contains the catalytic residue His263 does not have altered H/D-exchange properties upon iron addition (Fig. 5E). This may indicate that, in the absence of porphyrin substrate, iron binding does not affect the actual catalytic site, but may affect the positioning of the π-helix.

4. Discussion

Redox active metals such as iron are fundamental to many metabolic and regulatory pathways, yet the mechanism by which these metals are inserted into cofactors or proteins is only recently garnering attention. Ferrochelatase is one such enzyme whose activity was described as early as 1956 [35]; but only now, through the biochemical and structural research that is ongoing, are mechanistic details of the last step of heme synthesis becoming more defined [18]. The importance of this reaction to cellular function and human health is clear; defects in heme synthesis and metabolism can lead to severe developmental and health related effects. Decreased ferrochelatase activity can cause an accumulation of precursor porphyrins within cells which results in the disease protoporphyria [2,4]. An understanding of the mechanism of ferrochelatase is of key importance; however, there is controversy regarding the terminal acceptors of substrate iron and the residues which catalyze its insertion into protoporphyrin IX despite a multitude of crystal structures in the last decade. One of the main problems is that the crystallization conditions can influence the metal binding properties of ferrochelatase [8,9,11]. Several metals have been found to bind at more than one site [8,9,11] and some postulate that the lack of metal binding to His263 in the human structure [7] was from blockage by the cholate detergent molecules in the active site [9]. While site directed mutagenesis studies and crystal structures provide much needed insight, they are not answering the lingering question: how is iron transported to the active site and what structural features are involved?

Since static protein structures are often inadequate at describing the sometimes slight, yet crucial structural changes required for enzymatic processes, a measurement of protein dynamics can provide more insight into the mechanism of ferrochelatase [14]. To understand the protein structure–function relationship of ferrochelatase, it is imperative to localize the regions of the enzyme that are changing upon iron binding in solution. Amide hydrogen/deuterium exchange mass spectrometry was used to map these changes by comparing the deuterium incorporation rates into the backbone of apo- and iron-ferrochelatase in the absence of porphyrin substrate. H/D exchange kinetics can vary dramatically within a protein due to hydrogen bonding, solvent accessibility, and backbone flexibility [27,28]. Therefore, the amide exchange rate is highly dependent on protein structure, as well as dynamics. With respect to ferrochelatase, the rate of amide hydrogen exchange will provide essential information for understanding the mechanism of iron binding by localizing the dynamic processes the enzyme undergoes. Even though the current kinetic scheme has PPIX binding before Fe(II), PPIX was absent from the ferrochelatase preparation so that the effects of metal binding can be discerned without interference from enzyme turnover which is likely to involve different conformational changes.

The relative solvent (*i.e.*, D_2O) accessibility of apo-ferrochelatase is consistent with the 2 Å crystal structure of the human enzyme in the absence of protoporphyrin [7]. As shown in Fig. 3 (dark blue), the three prominent areas of protection are at the dimer interface formed by the α_{11} helix (peptides 270–281 and 283–289), at the regions flanking [2Fe–2S] cluster (peptides 197–203 and 270–281), and within the protoporphyrin binding pocket (peptides 76–84, 189–194, and 197–203). Of the peptides identified, peptides 270–281 and 76–84 encompass the most protected regions of ferrochelatase based on deuterium exchange, with little to no

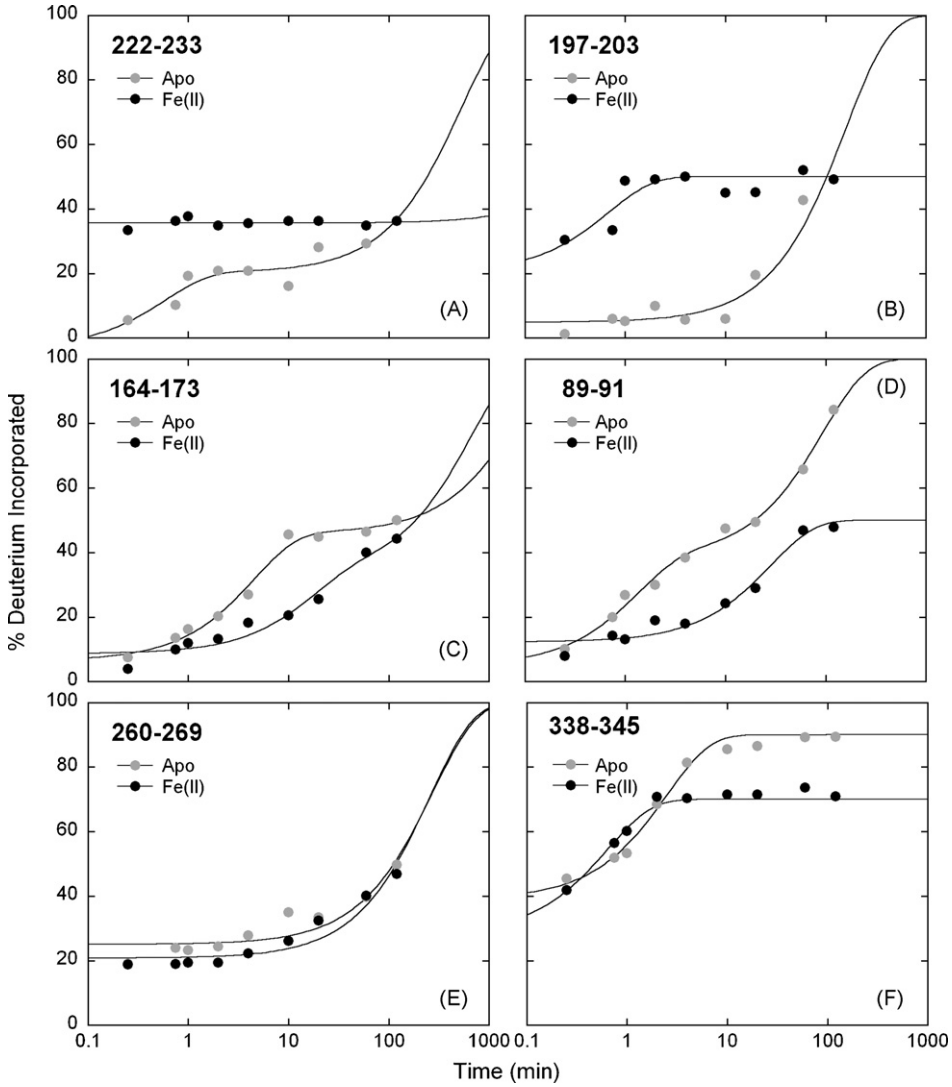

Fig. 5. H/D-exchange MS kinetic rate profiles for selected peptides. Shown are the kinetic traces for % deuterium incorporation into peptides derived from apo (gray spheres) and iron (black spheres) ferrochelatase as a function of incubation time in D_2O. The data are an average of two to three sets and were fit to single or double exponential equations (Eq. (2)) as appropriate. The fitted parameters are given in Table 1. (A) 222–233, (B) 197–203, (C) 164–173, (D) 89–91, (E) 260–269, and (F) 338–345. The kinetic profiles and fits for all peptides can be found in Supplementary Content (Figure S1).

deuterium incorporation over a 2 h incubation in D_2O (data not shown). Both peptides line one face the hydrophobic porphyrin binding pocket so the lack of solvent accessibility is not unexpected. Peptide 270–281 contains Tyr276 which is known to interact with protoporphyrin [10], although protoporphyrin is not present in the H/D-exchange MS studies. Residues within 270–281 are within 3.7 Å of the [2Fe–2S] cluster, which is conserved in mammalian and some bacterial enzymes. Peptide 76–84 is actually in a loop between the β_1 sheet and the α_1 helix. Despite being a loop which is typically dynamic, this region is highly inaccessible to deuterium to the same degree as peptide 270–280. Thus, the relative solvent inaccessibility and lack of dynamics in these regions may have functional importance to protoporphyrin binding. The lack of changes in H/D exchange behavior in the presence of iron supports this idea.

Although one face of the porphyrin binding pocket is not accessible to D_2O, the other face exchanges readily and includes peptides 93–101, 300–317, 338–345, and 352–356, which at 79% has the highest amount of deuterium incorporated after a 15 s incubation (Fig. 3C). Residues in these regions such as Leu98, Val305, and Trp110 are known to have direct interactions with protoporphyrin and many others are in van der Waals distance [10]. Since the H/D-exchange MS studies were performed in the absence of protoporphyrin and these residues are at the top part of the binding pocket known as the upper and lower "lips" (Fig. 3A), it is expected to have more deuterium incorporation here as compared to regions farther down the pocket. These lips are also the likely site for membrane association because of their hydrophobic residues and recent structures indicate that they can exist in "open" and "closed" conformations that may regulate protoporphyrin binding and product release through the membrane [15,31]. It may be that D_2O accessibility and H/D-exchange behavior in these areas may change when PPIX is bound before Fe(II) binds, as in the current accepted model [31].

Given the controversy regarding the pathway by which iron is transported to the active site, we were hopeful that H/D-exchange MS could shed light on the areas of ferrochelatase that are involved in this process. In the presence of iron, there are no dramatic changes to the ferrochelatase structure based on the H/D-exchange behavior of backbone amides (Fig. 3C), but some noteworthy differences were observed. The most obvious changes in deuterium incorporation occur for two peptides that are both highly resistant to exchange in the apo-enzyme (Fig. 5A and B). As shown in Fig. 4,

peptide 222–233 is located on the surface of ferrochelatase 20–30 Å away from the active site and peptide 197–203 is within 4–5 Å. The marked deuterium increase into the backbone of these segments can be attributed to a change in conformation upon iron binding at some region of the protein that alters the accessibility amides to D_2O.

In the human structure, Wu et al. [7] observed a Co(II) ion coordinated by matrix-exposed residues His231 and Asp383, which were postulated to be an initial metal binding site that leads into a channel to the active site. It is interesting that an increase in deuterium incorporation was observed for peptide 222–233, which contains His231. The data do not support the presence of a stable metal binding site in this region, where decreased dynamics might be expected as was observed for other metal binding sites in proteins [32,33]. However, it cannot be conclusively determined from the results whether iron is or is not coordinated by His231 (and Asp383 for which there was not peptide coverage). The H/D-exchange results do support that the region around His231 changes conformation in response to iron, which leads credence to the idea that this may be an entry point for the iron channel and not a stable binding site. Consistent with this, a H231A ferrochelatase mutant displayed an increased K_m for iron but still retained partial activity [34]. The adjacent peptide 197–203 forms part of the putative iron channel leading to the porphyrin binding site [7]. This region contains several polar amino acids such as Ser and Thr (^{197}STTGSSL^{203}), which could participate in transport (Fig. 4B) and Thr198 is within van der Waals distance to protoporphyrin. Also, Cys196, immediately before this fragment, coordinates one of the iron atoms of the [2Fe–2S] cluster. It appears as though this increase in solvent accessibility in this area is likely due to an opening of the channel in response to iron binding. Whether this channel is the actual path iron takes to the active site cannot be inferred from H/D-exchange behavior on its own, but it is clear that it is involved in some way.

Farther up the putative iron channel (Fig. 4B) peptides 164–173 and 89–91 incorporate less deuterium into the backbone in the iron-bound state (Fig. 5C and D). This change is not indicative of decreased solvent accessibility, but rather conformational change that leads to the formation of new hydrogen bonds or burial of amide hydrogens. Residues 164–173 form a loop on one side of the active site pocket which has extensive hydrogen bonding to both 197–203 and 89–91 in the apo-ferrochelatase structure [7]. For example, Arg164 (peptide 164–173) hydrogen bonds to Ser201 (peptide 197–203) and Arg91 (peptide 89–91) forms a hydrogen bond with Tyr165 (peptide 164–175). Thus, functional conformational changes in any of these regions upon iron binding are likely to be transmitted through hydrogen-bonds to the other sites. Mutational analysis of residues in these areas clearly indicates some involvement in the metallation step [7,34]. Sellers et al. [34] have proposed that Arg164 and Tyr165 are both terminal ligands for iron before insertion into the porphyrin substrate based on the increased K_m for iron in the R164L and Y165F mutants. The H/D exchange kinetic profile of 164–173, which shows decreased dynamics in iron-bound ferrochelatase, could indicate some involvement in iron coordination. The H/D exchange protection of one backbone amide in fragment 89–91 may be the result of changes in hydrogen bonding with fragment 164–173 if iron is interacting with amino acids in the region. It seems unlikely given the amino acid side chains (^{89}LLR^{91}) that peptide 89–91 is contributing to iron coordination in this manner, although backbone coordination cannot be ruled out.

The available ferrochelatase crystal structures show that the conserved His263 in the active site (Fig. 4B, red) is positioned with its side chain facing one side of the porphyrin macrocycle [10,11,36]. Two mechanisms exist for the role of His263, and there are biochemical, biophysical, and structural evidence to support both hypotheses. Hypothesis 1 has His263 and Glu343 as terminal ligands for iron which is then inserted into porphyrin from the same face as His263 [11]. Hypothesis 2 has metallation occurring from Arg164 and Tyr165 on the opposite site of His263 which abstracts two pyrrole protons that exit via Glu343 and other residues in the π-helix [12]. Site-directed mutants of His263 have no measurable activity [12] and this strongly suggests that regardless of whether it is an iron ligand or not, its role is key to catalysis.

The controversy as to whether the iron is inserted into protoporphyrin via His263 or by residues on the opposite side may not be solved by H/D-exchange MS, but this study clearly indicates that the region surrounding His263 (peptide 260–269) does not experience changes in backbone conformation or solvent accessibility in the presence of iron (Fig. 5E). This peptide spans a loop and most of the α_{10} helix. If His263 is a ligand, it should be accessible to bind iron in the absence of protoporphyrin. The H/D exchange results for 260–269 indicate that backbone amides lack of solvent accessibility and dynamic motions in both apo- and iron-ferrochelatase. Iron coordination to the His263 side chain and other residues in a binding site should give decreased dynamic motions in this loop region which was not observed. This suggests that iron may not stably bind to residues in this section of ferrochelatase, which disfavors hypothesis 1 [11]. Glu343, the other potential ligand in hypothesis 1, is part of peptide 338–345 (Fig. 4B). This peptide exhibits decreased dynamics in the presence of iron (Fig. 5F) which could be consistent with iron binding in hypothesis 1. However, the second hypothesis claims that residues along the π-helix are involved in abstracting two protons from the porphyrin substrate and shuttling them away from the active site [12,31]. It could be that metal binding on the other side of the active site, as purported in hypothesis 2, could affect dynamics in the π-helix. A third possibility could be that iron is binding at a secondary site formed by His, Glu, and Asp residues on the π-helix surface. In fact, crystals of bacterial and yeast ferrochelatases soaked with various metals have shown that iron can readily bind to these conserved residues which lead to the early hypothesis that they bound and shuttled iron to the active site [9,11,37]. Mutagenesis of these residues (D340E, E343D and H341C) result in diminished activity without a significant change in K_m for either iron or protoporphyrin [12]. These data do not support a role in metallation since the relative affinity of ferrochelatase for iron was not altered. It seems reasonable that the 1.5 molar equivalents of iron added to ferrochelatase for H/D-exchange MS could lead to secondary binding at this acidic site, but that it is unlikely to be physiologically relevant. The H/D-exchange data, taken together with mutagenesis and structural data, give more credence to the second hypothesis which has the terminal iron acceptors before insertion at or near Arg164 and Tyr165, and not His 263.

5. Conclusions

For the first time, it is demonstrated how the binding of iron affects the structure of ferrochelatase in solution. Through H/D-exchange mass spectrometry, we have mapped a structural response to iron which provides insight into the mechanism by which iron is transported to the active site. Our data support an iron-responsive channel from the surface of the enzyme towards the active site pocket where protoporphyrin binds, much like that previously proposed (Fig. 4B). In the active site of ferrochelatase, residues on the side of the pocket opposite the key catalytic residue His263 are most likely involved in the formation of a terminal iron binding site. In addition, the H/D-exchange data reveal that iron does not induce structural changes around the key catalytic residue and possible iron ligand, His263.

Acknowledgements

This work was supported by the National Science Foundation award #0845273 (to L.S.B.) and by the Ronald E. McNair Post-Baccalaureate Achievement Program (McNair Scholars) of The University of Alabama, U.S. Department of Education TRIO grant P217A030031 (to A.P.A). The authors thank Dr. Harry Dailey (The University of Georgia) for supplying the plasmid containing the ferrochelatase gene and for helpful discussions. We also thank Dr. Patrick Frantom for his assistance generating PyMol movies.

Appendix A. Supplementary data

Supplementary data associated with this article can be found, in the online version, at doi:10.1016/j.ijms.2010.08.004.

References

[1] H.A. Dailey, T.A. Dailey, Ferrochelatase, in: K.M. Kadish, K.M. Smith, R. Guilard (Eds.), The Porphyrin Handbook, Elsevier Science, 2003, pp. 93–121.
[2] I.A. Magnus, A. Jarrett, T.A. Prankerd, C. Rimington, Erythropoietic protoporphyria. A new porphyria syndrome with solar urticaria due to protoporphyrinaemia, Lancet 2 (1961) 448–451.
[3] F.P. Chen, H. Risheg, Y. Liu, J. Bloomer, Ferrochelatase gene mutations in erythropoietic protoporphyria: focus on liver disease, Cell Mol. Biol. (Noisy-le-grand) 48 (2002) 83–89.
[4] S. Sassa, G.L. Zalar, M.B. Poh-Fitzpatrick, K.E. Anderson, A. Kappas, Studies in porphyria: functional evidence for a partial deficiency of ferrochelatase activity in mitogen-stimulated lymphocytes from patients with erythropoietic protoporphyria, J. Clin. Invest. 69 (1982) 809–815.
[5] H.A. Dailey, M.G. Finnegan, M.K. Johnson, Human ferrochelatase is an iron-sulfur protein, Biochemistry 33 (1994) 403–407.
[6] H.A. Dailey, T.A. Dailey, C.K. Wu, A.E. Medlock, K.F. Wang, J.P. Rose, B.C. Wang, Ferrochelatase at the millennium: structures, mechanisms and [2Fe–2S] clusters, Cell Mol. Life Sci. 57 (2000) 1909–1926.
[7] C.K. Wu, H.A. Dailey, J.P. Rose, A. Burden, V.M. Sellers, B.C. Wang, The 2.0 Å structure of human ferrochelatase, the terminal enzyme of heme biosynthesis, Nat. Struct. Biol. 8 (2001) 156–160.
[8] D. Lecerof, M. Fodje, A. Hansson, M. Hansson, S. Al-Karadaghi, Structural and mechanistic basis of porphyrin metallation by ferrochelatase, J. Mol. Biol. 297 (2000) 221–232.
[9] T. Karlberg, D. Lecerof, M. Gora, G. Silvegren, R. Labbe-Bois, M. Hansson, S. Al-Karadaghi, Metal binding to Saccharomyces cerevisiae ferrochelatase, Biochemistry 41 (2002) 13499–13506.
[10] A. Medlock, L. Swartz, T.A. Dailey, H.A. Dailey, W.N. Lanzilotta, Substrate interactions with human ferrochelatase, Proc. Natl. Acad. Sci. U.S.A. 104 (2007) 1789–1793.
[11] M.D. Hansson, T. Karlberg, M.A. Rahardja, S. Al-Karadaghi, M. Hansson, Amino acid residues His183 and Glu264 in Bacillus subtilis ferrochelatase direct and facilitate the insertion of metal ion into protoporphyrin IX, Biochemistry 46 (2007) 87–94.
[12] H.A. Dailey, C.K. Wu, P. Horanyi, A.E. Medlock, W. Najahi-Missaoui, A.E. Burden, T.A. Dailey, J. Rose, Altered orientation of active site residues in variants of human ferrochelatase. Evidence for a hydrogen bond network involved in catalysis, Biochemistry 46 (2007) 7973–7979.
[13] G.C. Ferreira, R. Franco, A. Mangravita, G.N. George, Unraveling the substrate-metal binding site of ferrochelatase: an X-ray absorption spectroscopic study, Biochemistry 41 (2002) 4809–4818.
[14] L.S. Busenlehner, R.N. Armstrong, Insights into enzyme structure and dynamics elucidated by amide H/D exchange mass spectrometry, Arch. Biochem. Biophys. 433 (2005) 34–46.
[15] A.E. Medlock, M. Carter, T.A. Dailey, H.A. Dailey, W.N. Lanzilotta, Product release rather than chelation determines metal specificity for ferrochelatase, J. Mol. Biol. 393 (2009) 308–319.
[16] Z. Shi, G.C. Ferreira, Probing the active site loop motif of murine ferrochelatase by random mutagenesis, J. Biol. Chem. 279 (2004) 19977–19986.
[17] B. Szefczyk, M.N. Cordeiro, R. Franco, J.A. Gomes, Molecular dynamics simulations of mouse ferrochelatase variants: what distorts and orientates the porphyrin? J. Biol. Inorg. Chem. 14 (2009) 1119–1128.
[18] S. Al-Karadaghi, R. Franco, M. Hansson, J.A. Shelnutt, G. Isaya, G.C. Ferreira, Chelatases: distort to select? Trends Biochem. Sci. 31 (2006) 135–142.
[19] A.E. Burden, C. Wu, T.A. Dailey, J.L. Busch, I.K. Dhawan, J.P. Rose, B. Wang, H.A. Dailey, Human ferrochelatase: crystallization, characterization of the [2Fe–2S] cluster and determination that the enzyme is a homodimer, Biochim. Biophys. Acta 1435 (1999) 191–197.
[20] R.R. Loo, N. Dales, P.C. Andrews, The effect of detergents on proteins analyzed by electrospray ionization, Methods Mol. Biol. 61 (1996) 141–160.
[21] R.R. Loo, N. Dales, P.C. Andrews, Surfactant effects on protein structure examined by electrospray ionization mass spectrometry, Protein Sci. 3 (1994) 1975–1983.
[22] W. Najahi-Missaoui, H.A. Dailey, Production and characterization of erythropoietic protoporphyric heterodimeric ferrochelatases, Blood 106 (2005) 1098–1104.
[23] K.R. Clauser, P. Baker, A.L. Burlingame, Role of accurate mass measurement (±10 ppm) in protein identification strategies employing MS or MS/MS and database searching, Anal. Chem. 71 (1999) 2871–2882.
[24] Z. Zhang, A.G. Marshall, A universal algorithm for fast and automated charge state deconvolution of electrospray mass-to-charge ratio spectra, J. Am. Soc. Mass Spectrom. 9 (1998) 225–233.
[25] Z. Zhang, D.L. Smith, Determination of amide hydrogen exchange by mass spectrometry: a new tool for protein structure elucidation, Protein Sci. 2 (1993) 522–531.
[26] H.A. Dailey, Terminal steps of haem biosynthesis, Biochem. Soc. Trans. 30 (2002) 590–595.
[27] Y. Bai, J.S. Milne, L. Mayne, S.W. Englander, Primary structure effects on peptide group hydrogen exchange, Proteins 17 (1993) 75–86.
[28] R.S. Molday, S.W. Englander, R.G. Kallen, Primary structure effects on peptide group hydrogen exchange, Biochemistry 11 (1972) 150–158.
[29] K. Dharmasiri, D.L. Smith, Mass spectrometric determination of isotopic exchange rates of amide hydrogens located on the surfaces of proteins, Anal. Chem. 68 (1996) 2340–2344.
[30] D.L. Smith, Y. Deng, Z. Zhang, Probing the non-covalent structure of proteins by amide hydrogen exchange and mass spectrometry, J. Mass Spectrom. 32 (1997) 135–146.
[31] A.E. Medlock, T.A. Dailey, T.A. Ross, H.A. Dailey, W.N. Lanzilotta, A pi-helix switch selective for porphyrin deprotonation and product release in human ferrochelatase, J. Mol. Biol. 373 (2007) 1006–1016.
[32] C.E. Bobst, M. Zhang, I.A. Kaltashov, Existence of a noncanonical state of iron-bound transferrin at endosomal pH revealed by hydrogen exchange and mass spectrometry, J. Mol. Biol. 388 (2009) 954–967.
[33] M. Golynskiy, S. Li, V.L. Woods Jr., S.M. Cohen, Conformational studies of the manganese transport regulator (MntR) from Bacillus subtilis using deuterium exchange mass spectrometry, J. Biol. Inorg. Chem. 12 (2007) 699–709.
[34] V.M. Sellers, C.K. Wu, T.A. Dailey, H.A. Dailey, Human ferrochelatase: characterization of substrate-iron binding and proton-abstracting residues, Biochemistry 40 (2001) 9821–9827.
[35] H. Ashenbrucker, G.E. Cartwright, A. Goldberg, M.M. Wintrobe, Studies on the biosynthesis of heme in vitro by avian erythrocytes, Blood 11 (1956) 821–833.
[36] T. Karlberg, M.D. Hansson, R.K. Yengo, R. Johansson, H.O. Thorvaldsen, G.C. Ferreira, M. Hansson, S. Al-Karadaghi, Porphyrin binding and distortion and substrate specificity in the ferrochelatase reaction: the role of active site residues, J. Mol. Biol. 378 (2008) 1074–1083.
[37] D. Lecerof, M.N. Fodje, R. Alvarez Leon, U. Olsson, A. Hansson, E. Sigfridsson, U. Ryde, M. Hansson, S. Al-Karadaghi, Metal binding to Bacillus subtilis ferrochelatase and interaction between metal sites, J. Biol. Inorg. Chem. 8 (2003) 452–458.
[38] W.L. DeLano, The PyMOL molecular graphics system, DeLano Scientific, San Carlos, CA, 2002.